NJC

PAPER

View Article Online
View Journal | View Issue



Cite this: *New J. Chem.*, 2018, **42**, 13107

# Accelerated one-pot synthesis of coated magnetic nanoparticles from iron(II) as a single precursor

Jonathan Cruz-Vargas,[a] Fernando Belmont-Bernal,[a] César Gabriel Vera-De la Garza,[a] José Luis Pérez Mazariego,[b] Raúl Wayne Gómez González,[b] Laura Verónica Henao-Holguín,[c] Ivan Dario Rojas-Montoya[d] and Patricia Guadarrama *[a]

Received 9th May 2018,
Accepted 2nd July 2018

DOI: 10.1039/c8nj02270d

rsc.li/njc

In spite of the progress in synthetic methods to obtain nanoparticles, particularly magnetite either uncoated or coated, the implementation of easier, faster and reproducible protocols to obtain well-defined nanoparticles is still a challenge. In this work we present a one-pot approach to synthesize $Fe_3O_4$ nanoparticles uncoated and coated with dodecylamine (DDA), starting from a single iron precursor ($FeCl_2$) and incorporating a non-conventional stirring regime into the procedure. The products were characterized by XRD, TEM, TGA, FT-IR and Mössbauer spectroscopy, confirming the obtaining of the target materials. The magnetic measurements showed that the coated nanoparticles ($Fe_3O_4$@DDA) exhibited a higher saturation magnetization ($M_s$) and smaller coercivity ($H_c$) than the uncoated ones. The compromise between the saturation magnetization displayed by $Fe_3O_4$@DDA nanoparticles and the ease of its synthesis shows the potential of the method to obtain materials applicable to medical therapies.



## Introduction

One of the main challenges of nanoscience has been the development of easy and reproducible synthetic protocols to obtain nanostructures with well-defined composition for diverse applications like catalysis,[1,2] adsorption,[3,4] sensing,[5,6] optics,[7] and medical,[8–10] among others, where performance critically depends on the size and shape of the nanoparticles.

Among a variety of techniques, the liquid phase synthesis methods are by far the most used to synthesize nanomaterials.[11] In recent years such methods have advanced significantly, providing nanostructures of high purity and uniformity.

Particular attention has been given to the improvement of the synthesis methods to obtain magnetic iron oxide (generally, magnetite $Fe_3O_4$ and/or maghemite $\gamma$-$Fe_2O_3$) due to their diverse technological and biological applications such as contrast agents for Magnetic Resonance Imaging (MRI), carriers for drug delivery[12,13] or gene therapy,[14] therapeutic agents for hyperthermia based cancer treatments[15] and magnetic sensing probes for *in vitro* diagnostics (IVD).[16–18]

An assortment of chemical methods has been developed to synthesize magnetic/superparamagnetic iron oxide nanoparticles for diverse applications;[19] to mention some, the synthesis *via* microemulsions, sol–gel syntheses, sonochemical reactions, hydrothermal reactions, hydrolysis and thermolysis of precursors, high-temperature reactions, and electrospray syntheses.[20,21] Additionally, nanoprecipitation,[22,23] colloidal and polyol methods[24,25] have also been applied, with the possibility to incorporate surface coatings, both organic or inorganic, on the magnetic nanoparticles, as stabilizing agents to reduce aggregation but also to confer properties like stability against oxidation processes (see ref. 11), biocompatibility and hydrophilicity, crucial in the nanobiotechnology area. Generally, different nanoparticles can be coated in one of the following scenarios: *in situ*,[26] or post-synthesis,[27,28] accompanied in both cases by the narrowing of the size distribution.[29] The most common coatings are dextran, polyethylene glycol (PEG), polyvinyl alcohol (PVA), poloxamers, and poloxamines;[30,31] and other amines such as dodecylamine (DDA)[32,33] and amino-functional alkoxysilanes.[34]

Although the existing methods to synthesize nanoparticles have been optimized, some of them involve many phases, complicated purifications or multi-step processes with long reaction times, often under inert atmosphere conditions and elevated temperatures.[35]

[a] *Instituto de Investigaciones en Materiales, Laboratorio de Materiales Funcionales Orgánicos, Universidad Nacional Autónoma de México, Circuito Exterior s/n, Apdo. postal 70-360, Coyoacán, Ciudad de México, 04510, Mexico. E-mail: patriciagua@iim.unam.mx; Fax: +52-55-56161201; Tel: +52-55-56224594*
[b] *Facultad de Ciencias, Universidad Nacional Autónoma de México, Coyoacán, Ciudad de México, 04510, Mexico*
[c] *Facultad de Química, Departamento de Farmacia, Universidad Nacional Autónoma de México, Coyoacán, Ciudad de México, 04510, Mexico*
[d] *Facultad de Química, Departamento de Química Inorgánica y Nuclear, Universidad Nacional Autónoma de México, Coyoacán, Ciudad de México, 04510, Mexico*

In this article, we report a one-pot aqueous approach to synthesize coated $Fe_3O_4$ nanoparticles ($Fe_3O_4$@DDA), under stirring in a rotary evaporator, using dodecylamine (DDA) as a surface-functionalizing agent, and $FeCl_2$ as the single iron precursor. The reaction was carried out in five minutes, and an inert atmosphere was not needed since the dissolved oxygen is involved in the reaction. Similar protocols have been reported where the same Fe precursor was used, and mild reaction conditions were adopted[36,37] but the reaction times extend up to two hours.[38]

The synthetic method is reproducible and the resulting nanoparticles are stable and water-dispersible. Uncoated $Fe_3O_4$ nanoparticles were obtained under the same experimental conditions.

## Experimental section

### Materials

Iron(II) chloride tetrahydrate (98% m/m), dodecylamine 99% (DDA) and KOH pellets ($\geq$85%) were purchased from Sigma-Aldrich and were used without further purification. Ultrapure water (with a value of resistivity equal to 18.2 MΩ $cm^{-1}$ and 2 ppb of TOC (carbon–oxygen traces)) was used throughout the whole experiments.

### Instrumentation

The structure and average size particles of $Fe_3O_4$ and $Fe_3O_4$@DDA were determined by X-ray Powder Diffraction (XRD) with a Bruker AXS D8 Advance diffractometer. Transmission Electron Microscopy (TEM) observations were carried out in a JEM-ARM200F instrument (JEOL Japan), operating at 200 kV. Particle size distribution was measured by using ImageJ program.[39] Thermal stability of the nanoparticles was evaluated by thermogravimetric analysis (TGA) with a TA Instruments TGA Q500 IR with platinum tray, applying a heating rate of 10 °C $min^{-1}$ under $N_2$ and air atmosphere. Fourier Transform Infrared spectroscopy (FT-IR) spectra were obtained with a spectrometer Thermo Scientific Nicolet 6700. The magnetic properties were measured using a Physical Property Measurement System (PPMS) from Quantum Design, with a vibrating sample magnetometer (VSM) option and a home-made transverse susceptibility (TS) probe. The transmission Mössbauer spectroscopy was carried out using a $^{57}Co$ in rhodium source mounted in a constant acceleration spectrometer. Three spectra of the $Fe_3O_4$@DDA were taken in a powdered thin absorber (5 mg $cm^{-2}$) under different conditions: at room temperature and at 77 K in a home-made cryostat. To determine the effect of the DDA coating, a spectrum of synthesized $Fe_3O_4$ was also recorded. All the spectra were fitted with the Recoil program[40] and the reported isomer shifts are respect to α-Fe.

### Synthesis

**$Fe_3O_4$ nanoparticles.** 50 mL of a solution of $FeCl_2{\cdot}4H_2O$ (1.20 mM) in ultrapure water was prepared and then poured into a 200 mL ball-flask. To this solution was added KOH (1.8 mmol) and the mixture was placed without inert atmosphere or vacuum on a rotary evaporator at 245 rpm and heated at 90 °C for 5 minutes to obtain $Fe_3O_4$ nanoparticles as a black precipitate. The solid was decanted using a neodymium magnet and the nanoparticles were washed several times with water/acetone and then lyophilized.

**$Fe_3O_4$@DDA nanoparticles.** 50 mL of a solution of $FeCl_2{\cdot}4H_2O$ (1.20 mM) in ultrapure water was prepared and then poured into a 200 mL ball-flask containing an emulsion with 250 mg of DDA (1.34 mmol) and KOH (1.8 mmol) in ultra pure water. The mixture was placed without inert atmosphere or vacuum on a rotary evaporator at 245 rpm and heated at 90 °C for 5 minutes to obtain DDA coated $Fe_3O_4$ nanoparticles ($Fe_3O_4$@DDA) as a black precipitate. The solid was decanted using a neodymium magnet and the nanoparticles were washed several times with water/acetone and then lyophilized.

## Results and discussion

Commonly the obtaining of coated nanoparticles involves first the synthesis of the ''core'', followed by the coating with some material.[41] The synthetic method here reported allows to obtain magnetic nanoparticles, both coated and uncoated, in one step and in a reproducible way.

From XRD results, the presence of narrow and intense diffraction peaks demonstrated the crystallinity of the synthesized nanoparticles. According to the diffraction patterns (Fig. 1), regardless of the presence of DDA as a stabilizing agent, $Fe_3O_4$, and $Fe_3O_4$@DDA nanoparticles showed the same characteristic spinel structure of the magnetite (JCPDS 19-0629) with a principal reflection along (311) plane and none secondary phases.

Interestingly, also their average size range (10–30 nm) is similar. By the Scherrer equation,[42] the calculated average particle size was around 25 nm, which reasonably agrees with the microscopic measurements shown below. In terms of the average size, apparently not only the coating but also the

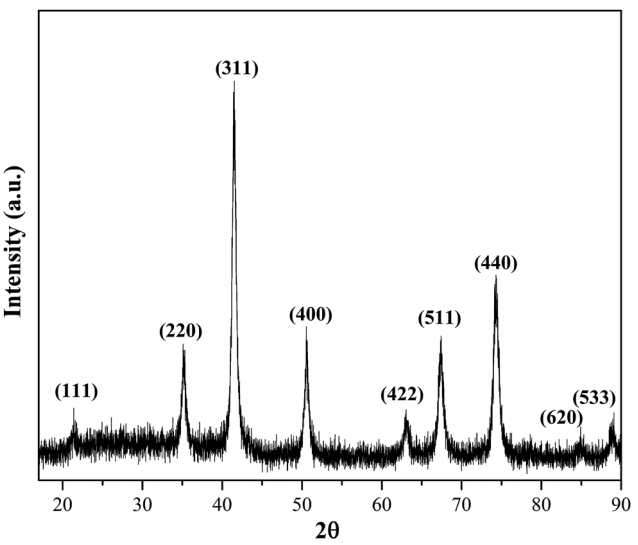


Fig. 1 XRD pattern analysis for $Fe_3O_4$@DDA nanoparticles (Kα Co = 1.7903 Å).

 

stirring regime by a rotary evaporator could be playing an important role since clearly differs from the conventional mechanical agitation that induces aggregation during the synthesis,[43] as well as the formation of a non-magnetic brown-red suspension of iron compounds,[44] thus affecting the reproducibility of some of the synthetic methods reported in the literature.[45]

Further studies will be conducted to get deep insight concerning the role of the stirring regime used in the present synthesis.

Transmission Electron Microscopy (TEM) revealed that uncoated magnetite nanoparticles ($Fe_3O_4$) shown in Fig. 2A, exhibit particle sizes between 11.8 and 26.1 nm, according to the histogram displayed in the inset of the figure.

In the case of $Fe_3O_4$@DDA coated nanoparticles (Fig. 2B) it can be seen that particle sizes are mostly around 20 and 35 nm, with an evident disaggregation, compared to the $Fe_3O_4$ sample, which is attributable to the DDA coating in the nanoparticle surface. High-resolution TEM of $Fe_3O_4$@DDA (Fig. 2C) clearly indicated the lattice fringes of the $Fe_3O_4$ core (*d* spacing = 2.94 Å), in one nanoparticle of around 26 nm. Moreover, the indexation of the diffraction pattern displayed the (220), (220) and (400) planes corresponding to the crystalline cubic spinel core of $Fe_3O_4$, which allows to the complete indexation of the remaining reflections. It is important to mention that the exhaustive analysis of several sections of the sample under study gave the same phase found in Fig. 2C. On the other hand, the *Z*-contrast image (Fig. 2D) exposes the coating, which it is estimated to be around 22.4 nm.

Thermogravimetric analyses (TGA) were carried out in air or nitrogen atmosphere for both $Fe_3O_4$@DDA and $Fe_3O_4$ magnetite nanoparticles previously lyophilized.

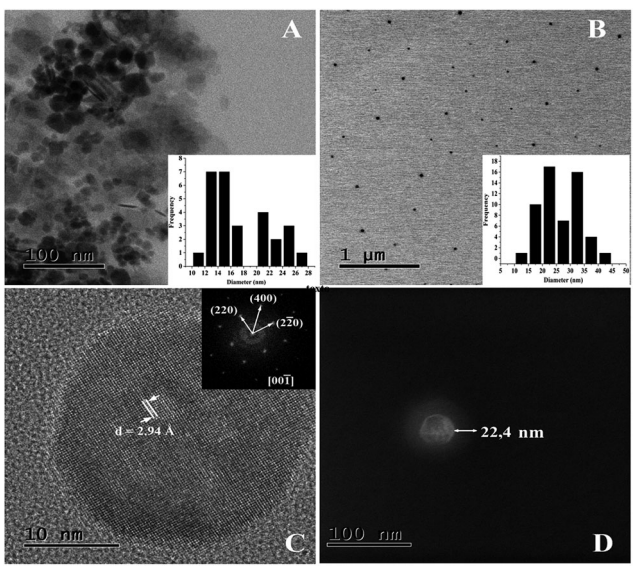


Fig. 2 TEM images, (A) $Fe_3O_4$ nanoparticles with histogram showing size distribution; (B) $Fe_3O_4$@DDA nanoparticles with histogram showing size distribution; (C) a high-resolution TEM image of a $Fe_3O_4$@DDA and the respective indexed diffraction pattern; (D) *Z*-contrast image of $Fe_3O_4$@DDA isolated indicating the length of DDA coating.

As shown in Fig. 3, the comparison between the samples $Fe_3O_4$ in air (black) and $Fe_3O_4$@DDA both in air (red) and in $N_2$ (blue), reinforces the TEM observation of the presence of DDA organic coating, with a degradation temperature range around 120–680 °C.

In red, 14.84% of mass, corresponding to the organic layer (DDA), is lost in a one-step pattern, while in blue, the first loss process corresponds to 9.27%, and the second to 9.02% of total mass. The uncoated sample $Fe_3O_4$/Air (black) was taken as a reference.

The weight loss observed in the range of 80–100 °C is related to the loss of water molecules that remain even after lyophilization of the samples, which demonstrates their structural nature. In the case of $Fe_3O_4$@DDA/Air, an abrupt loss of mass is detected between 145–360 °C which implies the degradation of organic layer by combustion due to the presence of atmospheric oxygen, under the experimental conditions.

The most interesting information comes from the TGA of $Fe_3O_4$@DDA/$N_2$ (blue). The organic layer weight loss shows a two-step degradation pattern, the first one between 155 and 400 °C and the second is registered from 400 to 680 °C, indicating that under an inert atmosphere, the pyrolysis degradation process is slow enough to detect the mass loss of DDA multilayers attached to the nanoparticle surface.

Both samples, $Fe_3O_4$ and $Fe_3O_4$@DDA were characterized by FT-IR, and the spectra are shown in Fig. 4.

The presence of magnetite core is verified by the two absorption bands above and below 500 $cm^{-1}$, corresponding to the Fe–O vibration. From the comparison of both FT-IR spectra, it is possible to demonstrate the presence of the organic coating in the $Fe_3O_4$@DDA sample *via* the bands around 2900 $cm^{-1}$, corresponding to the vibration of $-CH_2$ groups of DDA. In the region of 3250 $cm^{-1}$ is observed a broadband attributed to the vibration of O–H bonds from water molecules.

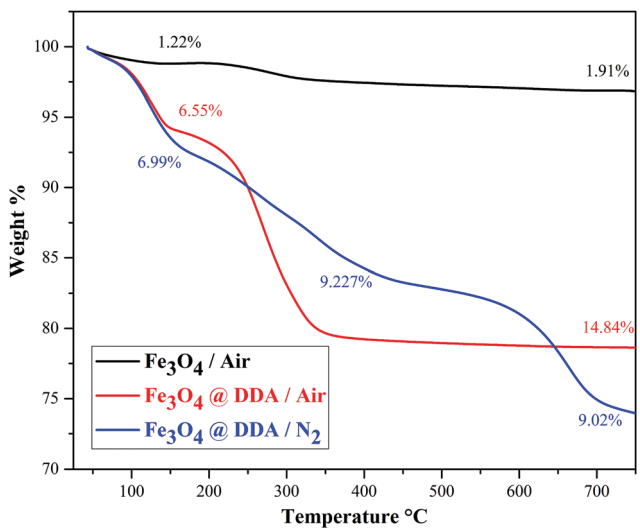


Fig. 3 Thermogravimetric analyses (TGA) of the samples $Fe_3O_4$@DDA/Air (red) and $Fe_3O_4$@DDA/$N_2$ (blue) previously lyophilized.

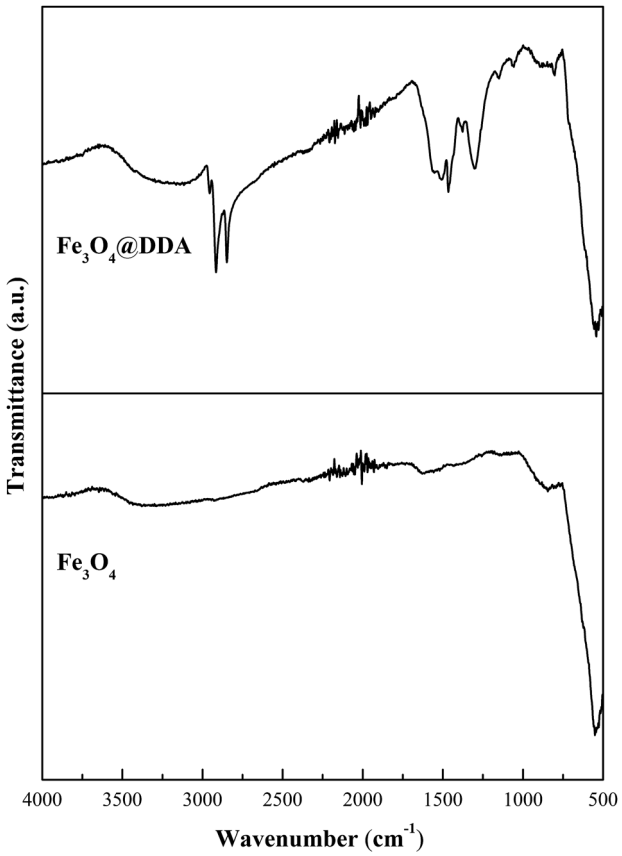


Fig. 4 FT-IR by ATR of magnetic nanoparticles $Fe_3O_4$ and $Fe_3O_4$@DDA.

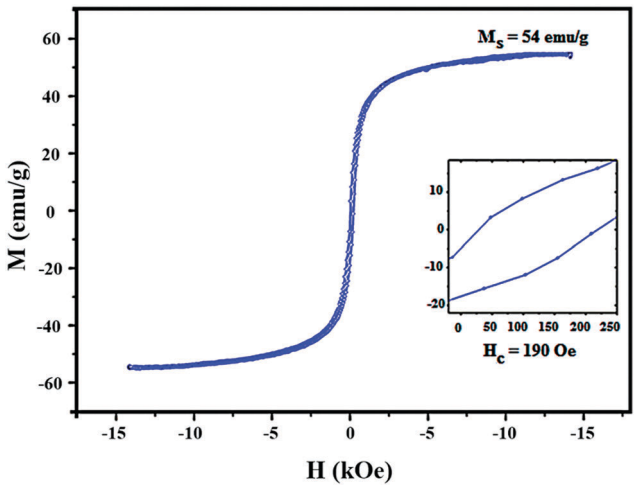


Fig. 5 Hysteresis loop analysis for $Fe_3O_4$. $M_s$ = 54 emu $g^{-1}$ and $H_c$ = 190 Oe.

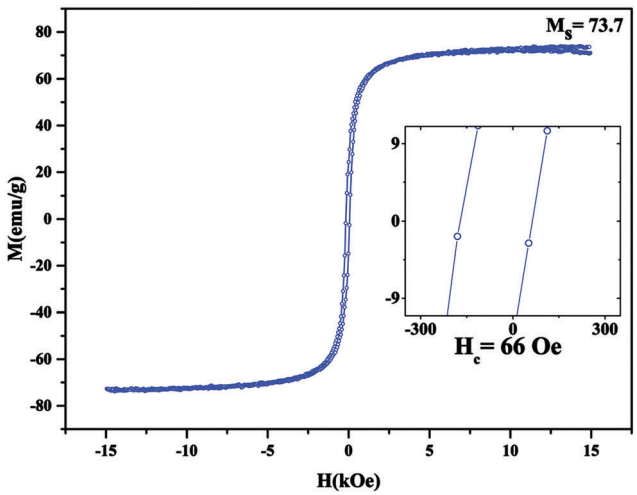


Fig. 6 Hysteresis loop analysis for $Fe_3O_4$@DDA. $M_s$ = 73.7 emu $g^{-1}$ and $H_c$ = 66 Oe.

Considering the magnetization as the most important property of the magnetite nanoparticles, zero-field-cooled/field-cooled (ZFC/FC) magnetization–temperature ($M$–$T$) curves were measured between 10 and 350 K, with $H$ = 50 Oe, while hysteresis loops, $M$–$H$, were measured at 50 and 300 K, applying fields up to $H$ = 50 kOe.

As a reference, the saturation magnetization for the sample $Fe_3O_4$ was measured. After the hysteresis loop was acquired, values of 54 emu $g^{-1}$ and 190 Oe were obtained for the saturation magnetization ($M_s$) and coercivity ($H_c$) respectively (Fig. 5). The relatively low value of $M_s$ can be associated with the agglomeration previously observed by TEM, which is a consequence of the strong magnetic dipole–dipole interaction,[46] that in turn is related with a decrease in heating efficiency[47] and becomes relevant when the hyperthermia is considered as a possible application.

The $Fe_3O_4$@DDA nanoparticles, on the other hand, exhibited a higher saturation magnetization ($M_s$ = 73.7 emu $g^{-1}$) than $Fe_3O_4$, with a lower coercivity ($H_c$ = of 66 Oe), as shown by the hysteresis cycle in Fig. 6, presumably because of the avoidance of agglomeration due to the presence of the coating, with chains long enough to correlate with better heating efficiencies.

The magnetization value achieved for $Fe_3O_4$@DDAis comparable to those observed for other coated magnetite nanoparticles synthesized by more elaborated methods.[48] According to the literature,[49,50] the existence of certain coercivity, like that exhibited by the sample $Fe_3O_4$@DDA, would not discard this material to be used in therapies such as hyperthermia.

To get deep insight into the magnetic behavior of the samples, the hyperfine magnetic fields were determined by Mössbauer spectroscopy. The spectrum of the $Fe_3O_4$ nanoparticles is displayed in Fig. 7A. It consists of two magnetic sextets (with a contribution of 90.3%), whose parameters correspond to magnetite (Table 1), and an apparent quadrupole doublet (with 9.7% contribution), probably attributable to a superparamagnetic behavior of smaller particles. It is interesting to note that when the nanoparticles are coated with DDA, the room temperature spectrum exhibits a noticeable doublet (a contribution of about 45%) due to particles whose sizes must be around 10 nm, and two smeared magnetic sextets (Fig. 7B and Table 2) associated with bigger (size $\geq$30 nm) nanoparticles.

The differences between these spectra can be explained by the inter-particle interactions when the nanoparticles are nearly in contact (uncoated sample).[51] In both cases, the blurriness of

 

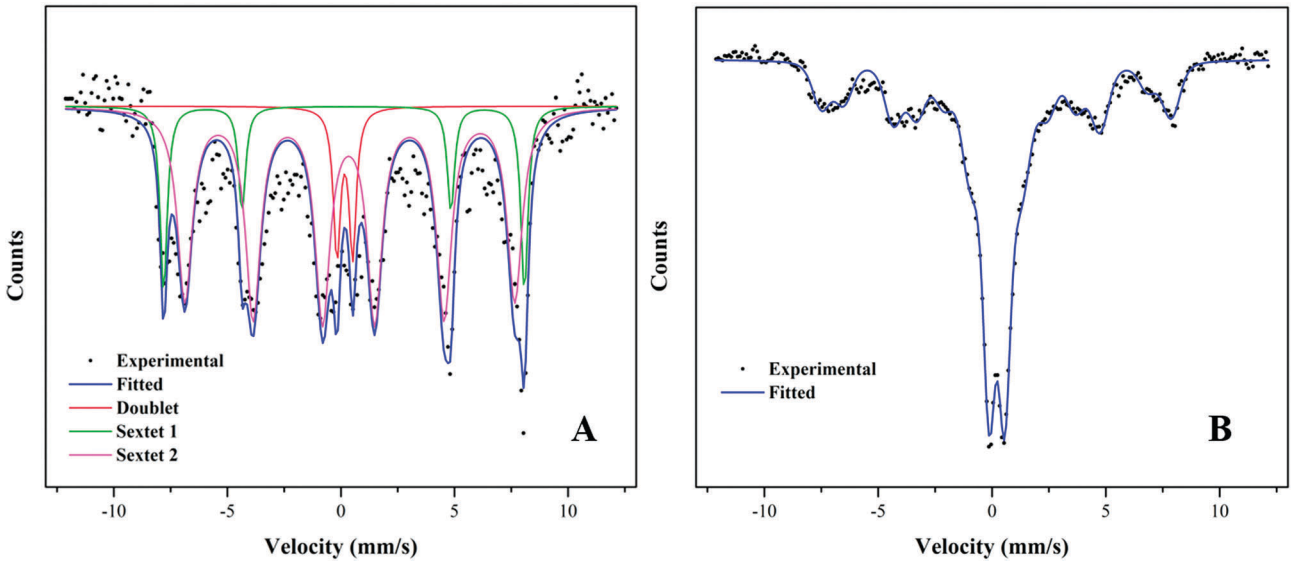


Fig. 7 Mössbauer spectra of (A) $Fe_3O_4$ and (B) $Fe_3O_4$@DDA nanoparticles.

Table 1 Mössbauer parameters of uncoated $Fe_3O_4$ nanoparticles

| Site parameters | $\delta$ (mm $s^{-1}$) | $\Delta Q$ (mm $s^{-1}$) | $H$ (T) | $\Gamma$ (mm $s^{-1}$) | % site populations |
|---|---|---|---|---|---|
| Doublet | 0.290 ± 0.031 | 0.704 ± 0.057 | | 0.19 | 9.7 ± 0.11 |
| Sextet 1 | 0.317 ± 0.021 | −0.057 ± 0.021 | 49.22 ± 0.14 | 0.19 | 20.7 ± 0.34 |
| Sextet 2 | 0.470 ± 0.020 | 0.015 ± 0.020 | 44.80 ± 0.20 | 0.35 | 69.6 ± 0.45 |

$\delta$ = isomer shift; $\Delta Q$ = quadrupole splitting; $\Gamma$ = line width.

Table 2 Mössbauer parameters of coated $Fe_3O_4$@DDA nanoparticles using the Voigt model

| Site parameters | $\delta$ (mm $s^{-1}$) | $\Delta Q$ (mm $s^{-1}$) | $H$ (T) | $\Gamma$ (mm $s^{-1}$) | $\sigma$ (mm $s^{-1}$) | % site population |
|---|---|---|---|---|---|---|
| Sextet 1 | 0.310 ± 0.01 | 0.003 ± 0.001 | 47.46 ± 0.07 | 0.19 | 0.30 | 25.3 ± 0.7 |
| Sextet 2 | 0.540 ± 0.01 | −0.057 ± 0.002 | 41.25 ± 0.07 | 0.19 | 0.30 | 29.4 ± 0.4 |
| Sextet 3 | 0.470 ± 0.002 | 0.015 ± 0.010 | 2.10 ± 0.08 | 0.19 | 0.18 | 44.8 ± 0.5 |

$\delta$ = isomer shift; $\Delta Q$ = quadrupole splitting; $\Gamma$ = line width, $\sigma$ gaussian width.

the sextets is caused by magnetic field distributions that arise from the different orientations of the single magnetic domains coupling between neighbor nanoparticles. In consequence, in the fitting processes, Voigt line shapes were used.[52,53]

To assure that the origin of the observed quadrupole doublet is due to a superparamagnetic behavior, a liquid nitrogen temperature spectrum was also recorded (Fig. 8 and Table 3) which is below the blocking temperature of magnetite nanoparticles of the average size estimated from the X-ray diffraction and TEM results. At those size nanoparticles, one should expect the normal magnetic behavior of magnetite (two differentiated sextets), however, the spectrum has clear signals of a superposition of the blurred sextets observed in the spectrum at room temperature, that is, the decoupling between single magnetic domains of the agglomerated nanoparticles is not completely broken at low temperature, and two new sextets associated with the nanoparticles below their blocking temperature are observed. Table 3 summarizes the parameters obtained under these conditions.

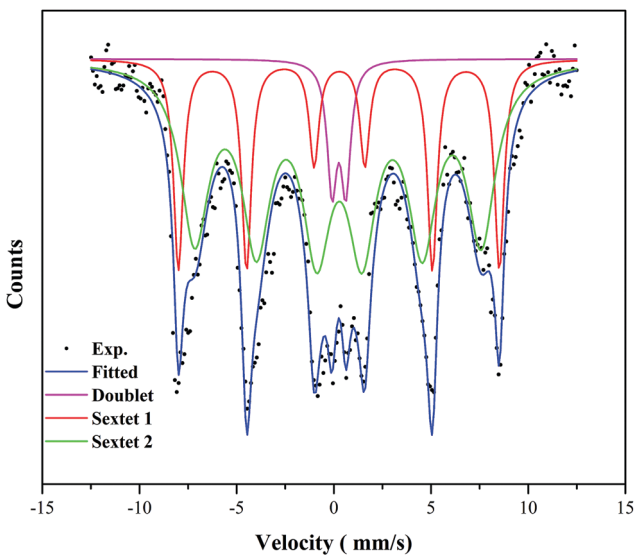


Fig. 8 Mössbauer spectrum of the $Fe_3O_4$@DDA nanoparticles at liquid nitrogen temperature.

Table 3 Mössbauer parameters of coated $Fe_3O_4$@DDA at liquid nitrogen temperature

| Site parameters | $\delta$ (mm s$^{-1}$) | $\Delta Q$ (mm s$^{-1}$) | $H$ (T) | $\Gamma$ (mm s$^{-1}$) | % site populations |
|---|---|---|---|---|---|
| Doublet | 0.382 ± 0.045 | 0.712 ± 0.072 | | 0.3 | 5.80 ± 0.54 |
| Sextet 1 | 0.394 ± 0.016 | −0.015 ± 0.016 | 51.21 ± 0.13 | 0.3 | 24.40 ± 0.18 |
| Sextet 2 | 0.368 ± 0.033 | −0.036 ± 0.030 | 45.72 ± 0.41 | 0.875 ± 0.047 | 69.80 ± 0.43 |

$\delta$ = isomer shift; $\Delta Q$ = quadrupole splitting; $\Gamma$ = line width.



One of the important facts to be noted is the unfolding of the collapsed sextet associated with the superparamagnetic behavior of the dispersed nanoparticles. In this scenario, a simple fitting process was done with Lorentzian profiles allowing large values of the line widths. Interestingly, the spectrum still shows a doublet, indicating the presence of nanoparticles whose dimensions are smaller than 10 nm.

Thus, the determinations by Mössbauer spectroscopy, particularly at low temperatures, allow us to understand the magnetic behavior of the $Fe_3O_4$@DDA nanoparticles in terms of the relatively low coercivity as a consequence of a certain degree of superparamagnetism which, as stated before, confers to this material a high potential in medical applications.

## Conclusions

Magnetic nanoparticles $Fe_3O_4$ and $Fe_3O_4$@DDA were obtained by a fast and reproducible method that incorporates a non-conventional stirring regime as an important parameter. The synthesis protocol allowed obtaining a homogeneous coating profile for $Fe_3O_4$@DDA nanoparticles, as was clearly observed by *Z*-contrast (HAADF) in TEM. According to TGA, DDA coating multilayer pattern were achieved, whose thermal degradation is related to their relative strength of interaction with the nanoparticles (inner and outer layers). FT-IR spectra corroborated the presence of both the coating and the structural water molecules. As noted by several authors, the presence of coatings like DDA in $Fe_3O_4$@DDA nanoparticles promotes high dispersability and deaggregation, which positively impacts properties like the average size and the magnetic behavior. From the magnetization measurements, the coated nanoparticles $Fe_3O_4$@DDA exhibited higher values of magnetization and lower coercivity, compared with the $Fe_3O_4$ sample. The compromise between the saturation magnetization displayed by $Fe_3O_4$@DDA nanoparticles ($M_s$ = 73.7 emu g$^{-1}$) and the ease of its synthesis, shows the potential of the method to obtain materials applicable in medical therapies.

From Mossbauer experiments, the following conclusions can be drawn; first, the noticeable difference between the spectra of coated and uncoated samples reconfirms the effectiveness of the DDA coating in the dispersion of the nanoparticles. Second, the remaining magnetism observed in the room temperature coated nanoparticles spectrum must be associated with a persisting fraction of agglomerated nanoparticles, presumably related with the formation of small clusters during the synthesis. Third, the spectrum acquired at liquid nitrogen temperature confirms that what seems to be a quadrupole doublet is actually a collapsed sextet, due to the superparamagnetic behavior of the nanoparticles. However, a minute doublet still presents manifesting that our sample contains a portion of particles smaller than 10 nm.

## Conflicts of interest

There are no conflicts to declare.

## Acknowledgements

Authors acknowledge Engineer Karla Eriseth Reyes Morales for her collaboration in the thermal analyses and MSc Adriana Tejeda Cruz for the analysis of the materials by X-ray diffraction and MSc Josué Romero-Ibarra for TEM observations. PG thanks to CONACyT and UNAM for financial support by the project 239672 and project 1316 respectively. JLPM and RWGG thanks to UNAM-DGAPA-PAPIIT Program IN114416.

## References

1 J. Wang and H. Gu, *Molecules*, 2015, **20**, 17070–17092.
2 B. R. Cuenya, *Thin Solid Films*, 2010, **518**, 3127–3150.
3 M. Habuda-Stanić and M. Nujić, *Environ. Sci. Pollut. Res.*, 2015, **22**, 8094–8123.
4 P. N. Dave and L. V. Chopda, *J. Nanotechnol.*, 2014, **2014**, 398569.
5 S. M. Ng, M. Koneswaran and R. Narayanaswamy, *RSC Adv.*, 2016, **6**, 21624–21661.
6 Y. Zhang, W. Chu, A. Foroushani, H. Wang, D. Li, J. Liu, C. Barrow, X. Wang and W. Yang, *Materials*, 2014, **7**, 5169–5201.
7 F. Iskandar, *Adv. Powder Technol.*, 2009, **20**, 283–292.
8 S. K. Murthy, *Int. J. Nanomed.*, 2007, **2**, 129–141.
9 M. R. Ghazanfari, M. Kashefi, S. F. Shams and M. R. Jaafari, *Biochem. Res. Int.*, 2016, **2016**, 7840161.
10 N. Sanvicens and M. P. Marco, *Trends Biotechnol.*, 2008, **26**, 425–433.
11 H. Goesmann and C. Feldmann, *Angew. Chem., Int. Ed.*, 2010, **49**, 1362–1395.
12 X. Mou, Z. Ali, S. Li and N. He, *J. Nanosci. Nanotechnol.*, 2015, **15**, 54–62.
13 S. Kakar, D. Batra, R. Singh and U. Nautiyal, *J. Acute Dis.*, 2013, **2**, 1–12.
14 C. Tang, P. J. Russell, R. Martiniello-Wilks, J. E. J. Rasko and A. Khatri, *Stem Cells*, 2010, **28**, 1686–1702.

 

15 Z. Hedayatnasab, F. Abnisa and W. M. A. W. Daud, *Mater. Des.*, 2017, **123**, 174–196.
16 G. Cordova, S. Attwood, R. Gaikwad, F. Gu and Z. Leonenko, *Nano Biomed. Eng.*, 2014, **6**, 31–39.
17 S. F. Hasany, N. H. Abdurahman, A. R. Sunarti and R. Jose, *Curr. Nanosci.*, 2013, **9**, 561–575.
18 J. Xie and S. Jon, *Theranostics*, 2012, **2**, 122–124.
19 U. Gozde, G. Ufuk, O. Ovidiu, F. Denisa, S. Maria, R. Marius, A. Mihaela and F. Anton, *Curr. Top. Med. Chem.*, 2015, **15**, 1622–1640.
20 S. Laurent, D. Forge, M. Port, A. Roch, C. Robic, L. Vander Elst and R. N. Muller, *Chem. Rev.*, 2008, **108**, 2064–2110.
21 R. A. Frimpong and J. Z. Hilt, *Nanomedicine*, 2010, **5**, 1401–1414.
22 S. F. Chin, S. C. Pang and S. H. Tay, *Carbohydr. Polym.*, 2011, **86**, 1817–1819.
23 C. Gavory, A. Durand, J.-L. Six, C. Nouvel, E. Marie and M. Leonard, *Carbohydr. Polym.*, 2011, **84**, 133–140.
24 E. Yamamoto, M. Kitahara, T. Tsumura and K. Kuroda, *Chem. Mater.*, 2014, **26**, 2927–2933.
25 K. J. Carroll, J. U. Reveles, M. D. Shultz, S. N. Khanna and E. E. Carpenter, *J. Phys. Chem. C*, 2011, **115**, 2656–2664.
26 H. Li, M. H. El-Dakdouki, D. C. Zhu, G. S. Abela and X. Huang, *Chem. Commun.*, 2012, **48**, 3385–3387.
27 K. Babu and R. Dhamodharan, *Nanoscale Res. Lett.*, 2009, **4**, 1090–1102.
28 R. Ghosh Chaudhuri and S. Paria, *Chem. Rev.*, 2012, **112**, 2373–2433.
29 Q. Zhang, J. Xie, J. Liang and J. Y. Lee, *Adv. Funct. Mater.*, 2009, **19**, 1387–1398.
30 Y. Zhang, N. Kohler and M. Zhang, *Biomaterials*, 2002, **23**, 1553–1561.
31 L. M. Lacava, Z. G. M. Lacava, M. F. Da Silva, O. Silva, S. B. Chaves, R. B. Azevedo, F. Pelegrini, C. Gansau, N. Buske, D. Sabolovic and P. C. Morais, *Biophys. J.*, 2001, **80**, 2483–2486.
32 H. Zhao, Z. Li, B. Yang, J. Wang and Y. Li, *J. Biomater. Sci., Polym. Ed.*, 2015, **26**, 1178–1189.
33 B. Sivaraman, C. A. Bashur and A. Ramamurthi, *Drug Delivery Transl. Res.*, 2012, **2**, 323–350.
34 R. A. Bini, R. F. C. Marques, F. J. Santos, J. A. Chaker and M. Jafelicci, *J. Magn. Magn. Mater.*, 2012, **324**, 534–539.
35 G. Saito and T. Akiyama, *J. Nanomater.*, 2015, **2015**, 123696.
36 M. Aslam, E. A. Schultz, T. Sun, T. Meade and V. P. Dravid, *Cryst. Growth Des.*, 2007, **7**, 471–475.
37 B. Bajaj, B. D. Malhotra and S. Choi, *Thin Solid Films*, 2010, **519**, 1219–1223.
38 S. A. Kahani and Z. Yagini, *Bioinorg. Chem. Appl.*, 2014, **2014**, 384984.
39 T. Wagner and J. Eglinger, *Zenodo*, 2017, thorstenwagner/ij-particlesizer: v1.0. 9 Snapshot release (version v1.0.9-SNAPSHOT).
40 K. Lagarec, Recoil 1.05., Mössbauer Analysis Software for Windows, 2002.
41 Y. Kobayashi, M. Horie, M. Konno, B. Rodríguez-González and L. M. Liz-Marzán, *J. Phys. Chem. B*, 2003, **107**, 7420–7425.
42 L. Alexander and H. P. Klug, *J. Appl. Phys.*, 1950, **21**, 137–142.
43 D. Li and R. B. Kaner, *J. Am. Chem. Soc.*, 2006, **128**, 968–975.
44 R. Valenzuela, M. C. Fuentes, C. Parra, J. Baeza, N. Duran, S. K. Sharma, M. Knobel and J. Freer, *J. Alloys Compd.*, 2009, **488**, 227–231.
45 R. Strobel and S. E. Pratsinis, *Adv. Powder Technol.*, 2009, **20**, 190–194.
46 P. L. Golas, S. Louie, G. V. Lowry, K. Matyjaszewski and R. D. Tilton, *Langmuir*, 2010, **26**, 16890–16900.
47 L. C. Branquinho, M. S. Carrião, A. S. Costa, N. Zufelato, M. H. Sousa, R. Miotto, R. Ivkov and A. F. Bakuzis, *Sci. Rep.*, 2013, **3**, 2887.
48 A. Kolhatkar, A. Jamison, D. Litvinov, R. Willson and T. Lee, *Int. J. Mol. Sci.*, 2013, **14**, 15977–16009.
49 A. J. Giustini, A. A. Petryk, S. M. Cassim, J. A. Tate, I. Baker and P. J. Hoopes, *Nano LIFE*, 2010, **01**, 17–32.
50 J. Motoyama, T. Hakata, R. Kato, N. Yamashita, T. Morino, T. Kobayashi and H. Honda, *Biomagn. Res. Technol.*, 2008, **6**, 4.
51 M. A. Polikarpov, V. M. Cherepanov, M. A. Chuev, S. Y. Shishkov and S. S. Yakimov, *J. Phys.: Conf. Ser.*, 2010, **217**, 012115.
52 D. G. Rancourt, *Nucl. Instrum. Methods Phys. Res., Sect. B*, 1989, **44**, 199–210.
53 D. G. Rancourt and J. Y. Ping, *Nucl. Instrum. Methods Phys. Res., Sect. B*, 1991, **58**, 85–97.